DOI: 10.61782/fa.2023.0386

forum acusticum 2023

THE NONLINEAR EIGENFREQUENCY PROBLEM OF ROOM ACOUSTICS WITH POROUS EDGE ABSORBERS

Florian Kraxberger[1,*] **Eniz Mušeljić**[1] **Eric Kurz**[2]
Florian Toth[3] **Manfred Kaltenbacher**[1] **Stefan Schoder**[1]
[1] Institute of Fundamentals and Theory in Electrical Engineering (IGTE), Graz University of Technology, Graz, Austria
[2] Signal Processing and Speech Communication Laboratory (SPSC), Graz University of Technology, Graz, Austria
[3] Institute of Mechanics and Mechatronics, TU Wien, Vienna, Austria

ABSTRACT

Using porous absorbers is common practice in the acoustic treatment of rooms. To reduce low-frequency reverberation in rooms, the absorber material is often placed in one or more edges of the room. Such an arrangement of porous absorbers is commonly known as bass trap or edge absorber. Edge absorbers have the advantage that, with relatively little porous absorber material, they efficiently reduce low-frequency reverberation, for which there are modal peaks in the room, and do not overattenuate high-frequency reverberation. A finite element model is employed to simulate the edge absorber's influence on a room's eigenfrequencies, wherein the edge absorber material is modeled using an equivalent fluid model. This results in a nonlinear eigenvalue problem due to the frequency dependence of the porous material parameters. The paper presents an iterative solution approach to the nonlinear eigenvalue problem and its application to acoustic predictions of edge absorbers. It is shown how edge absorbers shift and damp the eigenfrequencies of a room.

Keywords: *room acoustics, edge absorber, eigenvalue problem, JCAL model*

**Corresponding author*: *kraxberger@tugraz.at.*
***Copyright**: ©2023 Florian Kraxberger et al. This is an open-access article distributed under the terms of the Creative Commons Attribution 3.0 Unported License, which permits unrestricted use, distribution, and reproduction in any medium, provided the original author and source are credited.*

1. INTRODUCTION

Porous material (e.g., Basotect®) applied in the edge of a room has very good absorption properties in the low-frequency range, because it has a damping property at the room modes, which has been investigated empirically in [1–3]. This absorber type is often called bass trap or edge absorber (EA).

Simulation methods based on geometrical acoustics, conventionally used for room acoustics simulations, are not valid for low frequencies f and/or small geometric dimensions d [4, 5], i.e., the *Helmholtz* number $\mathrm{He} = 2\pi f d/c$ is much smaller than one. As a consequence, these simulation methods can not be used for low-frequency room acoustic simulations, from which the need for wave-based simulation methods arises. Okuzono *et al.* introduced a Finite Element (FE) model for room acoustic simulations with impedance boundary conditions (BCs) in [6]. Successively, their model was applied to simulate a large-scale auditorium [7]. Recently, a FE model for predicting the effect of EAs on the acoustic field in a room enclosed with sound-hard walls, as depicted in fig. 1, has been introduced [8]. This model is able to predict the influence of different configurations of EAs on the acoustic field, and has been validated using transfer function measurements in the reverberation chamber (RC) at Graz University of Technology. To model the porous material, the Equivalent Fluid Model (EFM) is used as defined in [9] and implemented in the open-

source FE software *openCFS* [1] [10, 11]. The frequency-dependent parameters of the EFM are the complex bulk modulus $K_{\mathrm{abs}}(\omega)$ and the complex (equivalent) density $\rho_{\mathrm{abs}}(\omega)$. They are defined by the Johnson-Champoux-Allard-Lafarge (JCAL) model [12], for which the material parameters are obtained with a fitting algorithm using impedance tube measurements, as described in [8, 13].

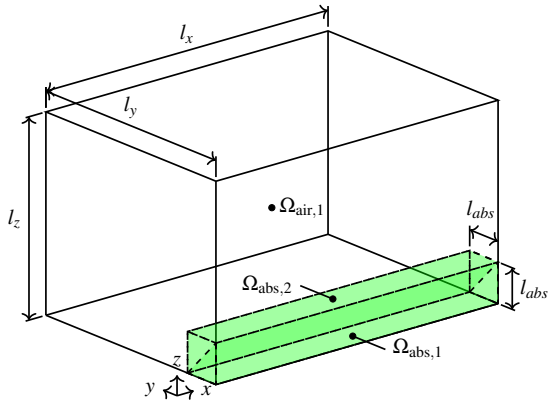

Figure 1. Sketch of geometry with air volume Ω_{air} and absorber volumes $\Omega_{\mathrm{abs},1}$ and $\Omega_{\mathrm{abs},2}$. The absorber volumes are colored green.

The frequency domain FE problem, as defined in [8], is to be solved with a maximum analysis frequency of 200 Hz. Investigations presented in [8] led to the conclusion that EAs influence the modal field by means of mode frequency shift and amplitude attenuation. Hence, in this article, the FE problem is reformulated into a *complex-valued nonlinear eigenfrequency problem* focusing on isolated low-frequency modes up to a frequency of approximately 100 Hz. The nonlinearity is caused by the frequency-dependent material parameters $K_{\mathrm{abs}}(\omega)$ and $\rho_{\mathrm{abs}}(\omega)$ of the EFM.

The proposed method can be used for real-world applications to determine the damped eigenfrequencies and the corresponding modal damping of a given EA configuration. Compared to running calculations of transfer functions (i.e., a harmonic analysis), the proposed method allows to evaluate modal damping values directly, whereas using harmonic simulations, the modal damping can only be determined indirectly, e.g. by comparing 3dB-bandwidths.

The paper is organized as follows. In sec. 2, the finite element model is described, the nonlinear eigenvalue (EV) problem is defined, and an iterative solution procedure is introduced. In sec. 3, the results of the nonlinear EV problem are documented. The article is concluded in sec. 4.

[1] https://opencfs.org/

2. METHODS

2.1 Geometry and Discretization

The geometry used for numerical simulations resembles the RC of the Laboratory of Building Physics at Graz University of Technology, which has edge lengths $l_x = 8.34\,\mathrm{m}$, $l_y = 5.99\,\mathrm{m}$, and $l_z = 4.90\,\mathrm{m}$. Along the longest axis of the RC, a porous material (melamine resin foam Basotect®) is placed, as depicted in fig. 1. In addition to the empty RC, and considering the cross-sectional area of the EA, three EA configurations are investigated: a square cross-section (EA1), a triangular cross-section pointing inwards (EA2), and a triangular cross-section pointing outward the RC (EA3). The investigated configurations are depicted in fig. 2.

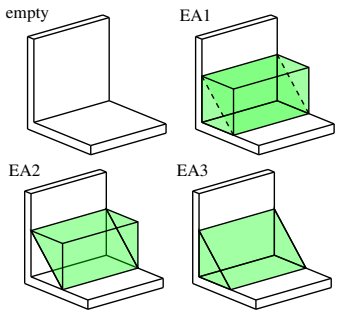

Figure 2. Simulation configurations empty, EA1, EA2, and EA3. The absorbent material is colored green.

The geometry is discretized using second-order Lagrangian elements. Due to the different wavelengths in air and the absorber medium (see [8, fig. 4]), a nonconforming mesh is used. A detailed view of the used mesh is depicted in fig. 3. The used element size corresponds to 6 elements per wavelength at the maximum analysis frequency of 200 Hz.

For the empty RC, the modal frequencies (i.e., the eigenfrequencies) can be computed using the analytical

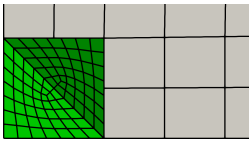

Figure 3. Detail view of the cross-section in the yz-plane through the nonconforming $\lambda/6$-mesh. The absorber volume is colored green, and the air volume is colored grey. [8, Fig. 5]

formula [14, p. 220]

$$f_{\text{mode,analyt}}^{(n_x,n_y,n_z)} = \frac{c_0}{2}\sqrt{\left(\frac{n_x}{l_x}\right)^2 + \left(\frac{n_y}{l_y}\right)^2 + \left(\frac{n_z}{l_z}\right)^2}\,, \quad (1)$$

where n_x, n_y, and n_z are the mode orders, and $c_0 = \sqrt{K_0/\rho_0}$ is the speed of sound in air. The modal frequencies are sorted in increasing order into the vector $\mathbf{f}_{\text{empty}}$.

2.2 Finite Element Formulation

The homogeneous wave equation of acoustic pressure p in a sound-hard room (i.e., homogeneous Neumann BCs at the enclosing surfaces) with the EFM is according to [9]

$$\frac{1}{K}\frac{\partial^2 p}{\partial t^2} - \nabla\cdot\frac{1}{\rho}\nabla p = 0\,. \quad (2)$$

Thereby, K is the bulk modulus, and ρ is the density. Introducing an isoparametric FE formulation [9,11] with the ansatz according to

$$w \approx w^h = \sum_i N_i w_i\,, \quad p \approx p^h = \sum_j N_j u_j\,, \quad (3)$$

where N are the FE basis functions, the wave equation in eq. (2) can be formulated in matrix-vector notation as

$$\boldsymbol{M}\frac{\partial^2}{\partial t^2}\boldsymbol{p} - \boldsymbol{K}\boldsymbol{p} = \boldsymbol{0}\,, \quad (4)$$

where $\boldsymbol{p}$ is the vector of degrees of freedom for (acoustic) pressure, and stiffness matrix $\boldsymbol{K}$ and mass matrix $\boldsymbol{M}$ are defined such that

$$\begin{aligned}\boldsymbol{M} &= \int_\Omega \frac{1}{K} w^h p^h \mathrm{d}\vec{x}\,,\\ \boldsymbol{K} &= \int_\Omega \nabla w^h\cdot\frac{1}{\rho}\nabla p^h \mathrm{d}\vec{x}\,.\end{aligned} \quad (5)$$

For acoustic pressure, the ansatz $p = \Re\{\tilde{p}\mathrm{e}^{st}\}$ is introduced, where s is a complex-valued free variable. This yields the *Helmholtz* problem in frequency domain, i.e.

$$\begin{aligned}\frac{s^2}{K}\tilde{p} - \nabla\cdot\frac{1}{\rho}\nabla\tilde{p} &= 0\,,\\ s^2\boldsymbol{M}\tilde{\boldsymbol{p}} - \boldsymbol{K}\tilde{\boldsymbol{p}} &= \boldsymbol{0}\,.\end{aligned} \quad (6)$$

The nonconforming interface between absorber and air volumes depicted in fig. 3 is handled using Nitsche-type mortaring, for which the FE formulation of the *Helmholtz* equation including appropriate interface terms is derived in [9]. Bulk modulus K and density ρ depend on location $\vec{x}$ and frequency ω, such that

$$\begin{aligned}K(\omega) &= \begin{cases}K_0 & \text{for } \vec{x}\in\Omega_{\text{air}}\\ K_{\text{abs}}(\omega) & \text{for } \vec{x}\in\Omega_{\text{abs}}\end{cases},\\ \rho(\omega) &= \begin{cases}\rho_0 & \text{for } \vec{x}\in\Omega_{\text{air}}\\ \rho_{\text{abs}}(\omega) & \text{for } \vec{x}\in\Omega_{\text{abs}}\end{cases}.\end{aligned} \quad (7)$$

Thereby, $K_0 = 141\,855\ \frac{\mathrm{N}}{\mathrm{m}^2}$ and $\rho_0 = 1.2305\ \frac{\mathrm{kg}}{\mathrm{m}^3}$ are the bulk modulus and density of air, and Ω_{air} and Ω_{abs} are the air and absorber volumes, respectively, according to the configurations defined in fig. 2.

2.3 JCAL Model for Porous Material

The equivalent bulk modulus $K_{\text{abs}}(\omega)$ and equivalent density $\rho_{\text{abs}}(\omega)$ from eq. (7) in the absorber volume are defined according to the JCAL model [12], such that

$$\begin{aligned}K_{\text{abs}}(\omega) &= \frac{\gamma p_0/\phi}{\gamma-(\gamma-1)\left[1-\mathrm{j}\frac{\kappa A'}{k_0' C_\mathrm{p}}\sqrt{1+\mathrm{j}\frac{4k_0'^2 C_\mathrm{p}}{\kappa\Lambda'^2\phi A'}}\right]^{-1}},\\ \rho_{\text{abs}}(\omega) &= \frac{\alpha_\infty\rho_0}{\phi}\left[1+\frac{\sigma A'}{\mathrm{j}\alpha_\infty}\sqrt{1+\mathrm{j}\frac{4\alpha_\infty^2\eta_0}{\sigma^2\Lambda^2\phi A'}}\right],\end{aligned} \quad (8)$$

where $A' = \phi/(\omega\rho_0)$, as well as the six parameters of the JCAL model, namely open porosity ϕ, static airflow resistance σ, high-frequency limit of the tortuosity α_∞, viscous characteristic length Λ, thermal characteristic length Λ', and static thermal permeability k_0'. Furthermore, the JCAL model needs parameters of air at measurement conditions, namely, dynamic viscosity $\eta_0 = 18.232\cdot10^{-6}\ \frac{\mathrm{kg}}{\mathrm{m\,s}}$, thermal conductivity $\kappa = 25.684\cdot10^{-3}\ \frac{\mathrm{W}}{\mathrm{m\,K}}$, isentropic exponent $\gamma = 1.4$, ambient air pressure $p_0 = 100\,325\,\mathrm{Pa}$, and specific heat of air at constant ambient pressure $C_\mathrm{p} = 1006.825\ \frac{\mathrm{J}}{\mathrm{kg\,K}}$ [8].

The six JCAL parameters are determined with a fitting procedure as documented in [13], where the result of the fitting procedure is listed in [8, tab. 1]. Equivalent bulk modulus $K_{\text{abs}}(\omega)$ and density $\rho_{\text{abs}}(\omega)$ as a result of the fitting procedure are depicted in fig. 4.

To quantify the degree of nonlinearity of the material parameters, one can expand the JCAL-model into a Taylor series around an expansion point $\omega_0 = 2\pi f_0$, which yields for $K_{\text{abs}}(\omega)$

$$K_{\text{abs}}(\omega) \approx \hat{K}_{\text{abs}}(\omega) = \sum_{i=0}^{N} (\omega - \omega_0)^i \underbrace{\frac{1}{i!} \frac{\partial^i K_{\text{abs}}(\omega)}{\partial \omega^i}\bigg|_{\omega_0}}_{a_i}, \tag{9}$$

and for $\rho_{\text{abs}}(\omega)$

$$\rho_{\text{abs}}(\omega) \approx \hat{\rho}_{\text{abs}}(\omega) = \sum_{i=0}^{N} (\omega - \omega_0)^i \underbrace{\frac{1}{i!} \frac{\partial^i \rho_{\text{abs}}(\omega)}{\partial \omega^i}\bigg|_{\omega_0}}_{b_i}. \tag{10}$$

Thereby, $\hat{\star}$ denotes the $(N-1)$-th order Taylor series approximation of $\star$. The complex-valued coefficients a_i of $\hat{K}_{\text{abs}}(\omega)$ and b_i of $\hat{\rho}_{\text{abs}}(\omega)$ have been computed using the *Matlab* function `taylor()` [15] and are listed in tab. 1. Using the EFM with the JCAL model results in frequency-dependent stiffness and mass matrices $\boldsymbol{K}(\omega)$ and $\boldsymbol{M}(\omega)$.

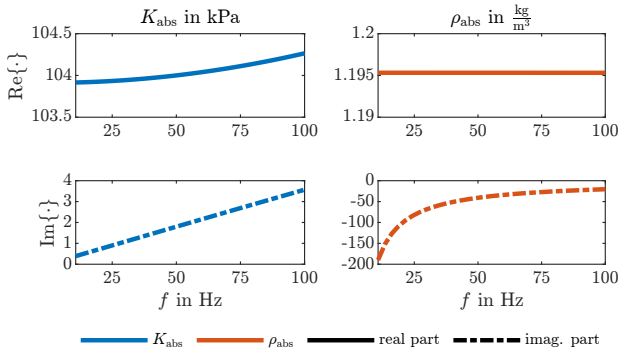

Figure 4. Real and imaginary parts of equivalent bulk modulus $K_{\text{abs}}(\omega)$ and density $\rho_{\text{abs}}(\omega)$.

2.4 Generalised Nonlinear EV Problem

From eq. (6), a generalized nonlinear EV problem can be formulated, such that

$$\boldsymbol{K}(\omega)\boldsymbol{p} = \lambda_k \boldsymbol{M}(\omega)\boldsymbol{p}\,, \tag{11}$$

where $\lambda_k = s_k^2$ are the sought EVs. The eigenvalue λ is complex-valued and can be written as (omitting the index k for better readability)

$$\begin{aligned} s &= -\omega_{\text{n}}\zeta \pm \text{j}\omega_{\text{n}}\sqrt{1-\zeta^2} = -\delta \pm \text{j}\omega_{\text{d}}\,, \\ \lambda = s^2 &= \underbrace{\omega_{\text{d}}^2 - \delta^2}_{-\alpha} \mp \text{j}\underbrace{2\delta\omega_{\text{d}}}_{-\beta}\,, \end{aligned} \tag{12}$$

where ω_{n} the undamped angular natural frequency, ω_{d} the damped angular frequency, δ is the decay constant, and $\zeta = \delta/\omega_{\text{n}}$ is the damping ratio. The values α and β are the results computed with *openCFS*. One can compute δ and ω_{d} from α and β with

$$\gamma = \frac{\alpha}{2} \pm \sqrt{\frac{\alpha^2}{4} - \frac{\beta^2}{4}}\,, \quad \delta = \pm\sqrt{\gamma}\,, \quad \omega_{\text{d}} = \frac{\beta}{2\delta}\,. \tag{13}$$

Decay constant δ and damped eigenfrequency ω_{d} are expected to be real-valued and positive; therefore, the set of equations (13) has a unique result. The corresponding damped eigenfrequency is $f = \omega_{\text{d}}/(2\pi)$. From δ and ω_{d}, the damping ratio ζ and ω_{n} can be computed as follows

$$r = \frac{-\delta}{\omega_{\text{d}}}\,, \quad \zeta = \sqrt{\frac{r^2}{1+r^2}}\,, \quad \omega_{\text{n}} = \frac{\omega_{\text{d}}}{\sqrt{1-\zeta^2}}\,. \tag{14}$$

The nonlinearity is due to the frequency dependence of stiffness and mass matrices $\boldsymbol{K}(\omega)$ and $\boldsymbol{M}(\omega)$, respectively, which is evident from the nonzero higher order Taylor series coefficients listed in tab. 1.

2.5 Iterative Solution Procedure

For the EV problem in eq. (11), an iterative solution procedure is introduced based on the fixed-point method. Let $\mathcal{F} : \mathbb{C}^2 \mapsto \mathbb{R}^{N_{\text{EV}}}$ denote the used FE system, which depends on the two complex-valued material parameters K and ρ, and maps to a N_{EV}-dimensional vector of eigenfrequencies. Considering a specific frequency ω_k, it maps the two complex values $K(\omega_k)$ and $\rho(\omega_k)$ to the vector of eigenfrequencies $\boldsymbol{f}_{\text{EV}}(\omega_k)$. Therefore, we can write

$$\boldsymbol{f}_{\text{EV}}(\omega_k) = \mathcal{F}\{K(\omega_k), \rho(\omega_k)\}\,, \tag{15}$$

which denotes one execution of the FE implementation in *openCFS* for one analysis frequency ω_k, at which the material properties are evaluated, resulting in a vector of eigenfrequencies $\boldsymbol{f}_{\text{EV}}(\omega_k)$.

In alg. 1, the algorithm used to solve the nonlinear EV problem is listed. It consists of an outer loop with index

Table 1. Taylor series coefficients a_i of $\hat{K}_{\text{abs}}(\omega)$ and b_i of $\hat{\rho}_{\text{abs}}(\omega)$ computed with the Matlab command `taylor()` for the expansion point $\omega_0 = 100\pi$ up to $N = 4$.

i	$\Re\{a_i\}$	$\Im\{a_i\}$	$\Re\{b_i\}$	$\Im\{b_i\}$
0	8.551	-8.832	1.058	-251.5
1	-0.1317	-71.66	0	1.601
2	$3.624 \cdot 10^{-2}$	$-9.599 \cdot 10^{-4}$	0	$-5.097 \cdot 10^{-3}$
3	$-2.284 \cdot 10^{-6}$	$2.074 \cdot 10^{-5}$	0	$8.112 \cdot 10^{-6}$
4	$-5.847 \cdot 10^{-9}$	$-5.661 \cdot 10^{-9}$	0	$-5.165 \cdot 10^{-9}$

k and an inner loop with index n. The outer loop iterates over the eigenfrequencies $\boldsymbol{f}_{\text{empty}}$ of the empty RC computed analytically using eq. (1), where the k-th element is used to initialize the inner loop with f_n. In the inner loop, the material parameters K and ρ are determined from the material model defined in eq. (8), evaluated for the k-th element in $\boldsymbol{f}_{\text{empty}}$. Therewith, the call to *openCFS* is denoted as $\mathcal{F}\{K, \rho\}$, which returns an eigenfrequency vector $\boldsymbol{f}_{\text{EV}}$. From $\boldsymbol{f}_{\text{EV}}$, the k-th element is stored in the element f_{n+1}. In addition to that, the imaginary part β corresponding to f_{n+1} is stored. The absolute deviation of f_{n+1} from f_n is the error e, i.e.

$$e = |f_{n+1} - f_n| \,. \tag{16}$$

If the error e is smaller than the stopping criterion ε, the algorithm is assumed to be converged (end of inner loop), and f_{n+1} is stored in the result vector $\boldsymbol{f}_{\text{empty}}$ at k-th position. An alternative stopping criterion is present when a maximum number of iterations N_{maxIt} is reached. Finally, the outer loop is restarted by selecting the $k+1$-th element of $\boldsymbol{f}_{\text{empty}}$.

Algorithm 1 is implemented using *PyCFS*, which is a Python interface to *openCFS* suited for automatization of *openCFS* calls [16]. For the solution of the generalized EV problem in *openCFS*, the eigenvalue solver *ARPACK* is used, which uses an Arnoldi-type method.

Algorithm 1: Iterative algorithm for the nonlinear EV problem.

Data: eigenfreq. of empty RC: $\boldsymbol{f}_{\text{empty}}$
Input: N_{EV}, N_{maxIt}, ε
Result: eigenfreq. of RC with EA: $\boldsymbol{f}_{\text{nlEV}}$

```
for k = 1, ..., N_EV do
    initialization: f_n ← f_empty[k];
    n ← 0;
    while e > ε and n ≤ N_maxIt do
        K ← K(2π f_n)          (eq. (8));
        ρ ← ρ(2π f_n)          (eq. (8));
        f_EV ← F{K, ρ}         (eq. (15));
        f_{n+1} ← f_EV[k];
        e ← |f_{n+1} − f_n|    (eq. (16));
        n ← n + 1;
    end
    f_nlEV[k] ← f_{n+1};
end
```

3. RESULTS

3.1 Eigenfrequencies of the RC with and without EA

Algorithm 1 is evaluated with the input parameters $N_{\text{EV}} = 25$, $N_{\text{maxIt}} = 10$, and $\varepsilon = 10^{-6}$ Hz. The maximum number of iterations necessary for the iterative solution procedure was five, hence the maximum iteration number stopping criterion was never reached. In tab. 2, the numerically evaluated eigenfrequencies are listed for the configurations depicted in fig. 2 up to the 25$^{\text{th}}$ eigenfrequency of the empty RC, which is approximately at 77.9 Hz when computed according to eq. (1). Note, that in tab. 2 for $k = 12$, the analytically computed eigenmode with the mode order $(n_x, n_y, n_z) = (1, 2, 0)$ could not be detected by the numerical scheme.

In fig. 5, the damping ratio ζ of the eigenmodes is depicted, and it can be deduced that up to $k \leq 13$, EA1 has the largest modal damping. For mode indices $k > 13$, larger fluctuations in ζ can be observed. Furthermore, the mode indices $k \in \{8, 14\}$ are highlighted, as for these mode indices, the field results are included in sec. 3.3. The mode at $k = 12$ is omitted because the iterative scheme did non converge to this mode.

Table 2. Mode orders, analytically and numerically computed eigenfrequencies of the empty RC, and numerically computed eigenfrequencies of EA1, EA2, and EA3.

k	mode order			analyt. eigenfreq. empty (in Hz)	numeric eigenfreq. (in Hz)			
	n_x	n_y	n_z		empty	EA1	EA2	EA3
1	1	0	0	20.36	20.36	20.28	20.31	20.32
2	0	1	0	28.34	28.34	28.34	28.30	28.32
3	0	0	1	34.65	34.65	34.66	34.60	34.63
4	1	1	0	34.89	34.89	34.84	34.81	34.84
5	1	0	1	40.18	40.18	40.16	40.10	40.14
6	2	0	0	40.71	40.71	40.60	40.62	40.64
7	0	1	1	44.76	44.76	44.88	44.65	44.74
8	1	1	1	49.17	49.17	49.23	49.01	49.11
9	2	1	0	49.61	49.61	49.49	49.43	49.49
10	2	0	1	53.46	53.46	53.37	53.30	53.36
11	0	2	0	56.68	56.68	56.76	56.60	56.68
12	1	2	0	60.23	—	—	—	—
13	2	1	1	60.51	60.51	60.45	60.21	60.36
14	3	0	0	61.07	61.07	60.94	60.92	60.97
15	0	2	1	66.43	66.43	66.69	66.32	66.48
16	3	1	0	67.32	67.32	67.17	67.04	67.17
17	0	0	2	69.29	69.29	69.40	69.18	69.31
18	1	2	1	69.48	69.48	69.71	69.34	69.50
19	2	2	0	69.79	69.79	69.80	69.63	69.74
20	3	0	1	70.21	70.21	70.07	69.96	70.07
21	1	0	2	72.22	72.22	72.31	72.09	72.22
22	0	1	2	74.86	74.86	75.12	74.69	74.92
23	3	1	1	75.72	75.72	75.55	75.26	75.49
24	1	1	2	77.58	77.58	77.81	77.38	77.62
25	2	2	1	77.92	77.92	78.08	77.69	77.89

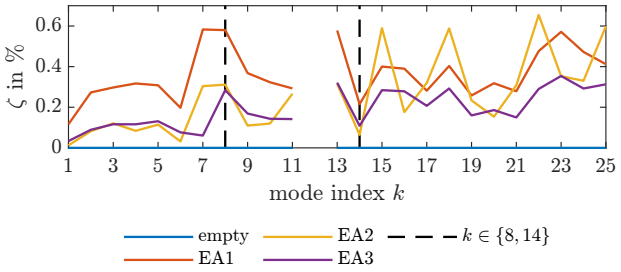

Figure 5. Damping ratio ζ of numerically evaluated eigenmodes.

3.2 Modal Assurance Criterion

To quantify how much the modes of the RC with EA (i.e., configurations EA1, EA2, and EA3) deviate from the modes of the empty RC, the modal assurance criterion (MAC) is used. It indicates how well modes (i.e., eigenvectors) of two different systems are matched [17], where one system is the empty RC, and the other system is one configuration with EA (see fig. 2). Thereby, only the air regions Ω_{air} are considered for the MAC. According to [17], the MAC can be computed with

$$MAC(m,n) = \frac{\left|\boldsymbol{\psi}_m^{\mathrm{T}} \boldsymbol{\chi}_n^*\right|^2}{\left(\boldsymbol{\psi}_m^{\mathrm{T}} \boldsymbol{\psi}_m^*\right)\left(\boldsymbol{\chi}_n^{\mathrm{T}} \boldsymbol{\chi}_n^*\right)} \cdot 100\,\%\,, \qquad (17)$$

where $\boldsymbol{\psi}_m$ is the eigenvector corresponding to the m-th eigenfrequency of the empty RC, and $\boldsymbol{\chi}_n$ is the eigenvector corresponding to the n-th eigenfrequency of one configuration with EA. Hence, the MAC matrices MAC_{EA1}, MAC_{EA2} and MAC_{EA3} are obtained. Furthermore, the AutoMAC matrix MAC_{empty} can be obtained by letting $\boldsymbol{\chi}_n$ be the eigenvectors of the empty RC.

The off-diagonal contributions of $MAC_{\text{empty}}(m,n)$, $MAC_{\text{EA1}}(m,n)$, $MAC_{\text{EA2}}(m,n)$ and $MAC_{\text{EA3}}(m,n)$,

i.e., where $m \neq n$, only provide insignificant contributions to the MAC. Hence, only the main diagonal, i.e. where $m = n$ is of interest. It is depicted in fig. 6, from which it is visible that the MAC is reduced for mode indices $k \geq 14$ for configurations EA1 and EA2, with the exception of mode $k = 19$. The mode at $k = 12$ is omitted because the iterative scheme did non converge to this mode.

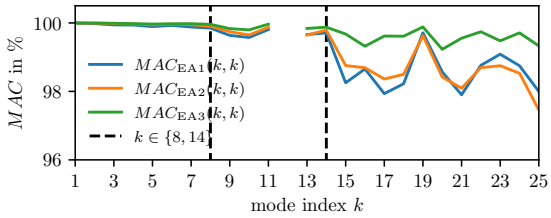

Figure 6. Main diagonal of MAC matrices, i.e. $MAC_{\mathrm{EA1}}(k,k)$, $MAC_{\mathrm{EA2}}(k,k)$, and $MAC_{\mathrm{EA3}}(k,k)$.

3.3 Modal Field Results

Figure 7 shows the numerically evaluated modal pressure field of the 8th eigenfrequency for the empty RC and all EA configurations, which corresponds to a mode order of $(n_x, n_y, n_z) = (1, 1, 1)$. In fig. 8, the numerically evaluated modal pressure field of the 14th eigenfrequency is depicted for the empty RC and all EA configurations, which corresponds to a mode order of $(n_x, n_y, n_z) = (3, 0, 0)$.

The difference in the pressure field between empty RC and the EA configurations is especially visible in the EA volume highlighted in green. However, also in the air volume, a significant damping of the pressure field can be observed, especially in fig. 7 showing the eigenmode for $k = 14$.

4. CONCLUSION

In this work, an iterative procedure for the nonlinear eigenfrequency problem arising in FE simulations with a porous material modeled as an equivalent fluid has been presented. This modeling method is superior to conventional simulation methods based on geometric acoustics because it models acoustic waves both in the air and absorber domains and is used for eigenvalue computations. The presented iterative procedure based on the fixed-point iteration is necessary due to the frequency-dependent material parameters of the EFM. From fig. 5, it is visible that

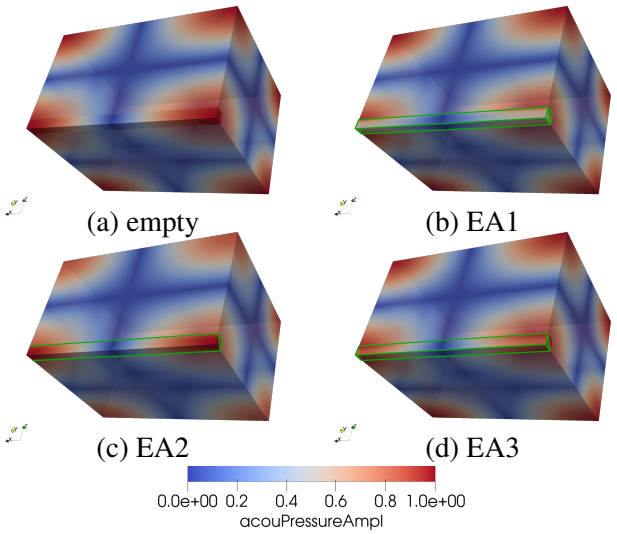

Figure 7. Field result for the numerically evaluated eigenvectors for $k = 8$ of (a) empty RC and (b)–(d) EA1, EA2, and EA3, respectively.

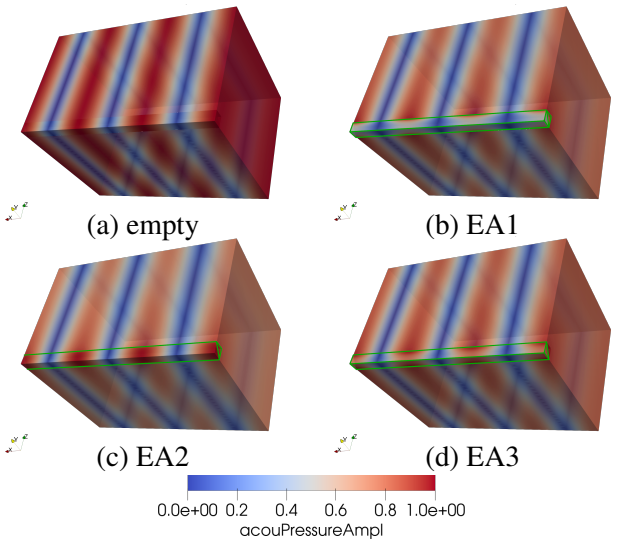

Figure 8. Field result for the numerically evaluated eigenvectors for $k = 14$ of (a) empty RC and (b)–(d) EA1, EA2, and EA3, respectively.

the damping property of EA is unevenly distributed across different modes. One presumption could be, that modes, for which $n_x \leq n_y + n_z$, have larger damping values than modes, for which the mode order inequality is not fulfilled (except for $k = 23$ and EA1 configuration). However, it is subject to further studies if this relation is also valid for other geometric arrangements (e.g., EA along the y-axis in the room).

5. ACKNOWLEDGMENTS

F. K. received funding from the Austrian Research Promotion Agency (FFG) under Bridge Project No. 39480417.

6. REFERENCES

[1] H. V. Fuchs and J. Lamprecht, "Covered broadband absorbers improving functional acoustics in communication rooms," *Appl. Acoust.*, vol. 74, no. 1, pp. 18–27, 2013.

[2] E. Kurz, D. Reisinger, W. Weselak, and G. Graber, "The edge absorber as a modal brake," in *Proc. of Forum Acusticum*, (Lyon, France), pp. 1745–1752, Dec. 2020.

[3] R. Hofer, "Analyse des modalen Schallfeldes zur Untersuchung der Funktionsweise von Kantenabsorbern (Analysis of the modal sound field to study the operation of edge absorbers)," Master's thesis, Graz University of Technology, 2022.

[4] M. Vorländer, "Computer simulations in room acoustics: Concepts and uncertainties," *J. Acoust. Soc. Am.*, vol. 133, no. 3, pp. 1203–1213, 2013.

[5] L. Savioja and U. P. Svensson, "Overview of geometrical room acoustic modeling techniques," *J. Acoust. Soc. Am.*, vol. 138, no. 2, pp. 708–730, 2015.

[6] T. Okuzono, T. Yoshida, K. Sakagami, and T. Otsuru, "An explicit time-domain finite element method for room acoustics simulations: Comparison of the performance with implicit methods," *Appl. Acoust.*, vol. 104, pp. 76–84, 2016.

[7] T. Yoshida, T. Okuzono, and K. Sakagami, "A parallel dissipation-free and dispersion-optimized explicit time-domain fem for large-scale room acoustics simulation," *Buildings*, vol. 12, no. 2, 2022.

[8] F. Kraxberger, E. Kurz, L. Merkel, M. Kaltenbacher, and S. Schoder, "Finite element simulation of edge absorbers for room acoustic applications," in *DAGA 2023*, (Hamburg), DEGA, Mar. 2023.

[9] M. Kaltenbacher and S. Floss, "Nonconforming finite elements based on nitsche-type mortaring for inhomogeneous wave equation," *J. Theor. Comput. Acoust.*, vol. 26, no. 03, p. 1850028, 2018.

[10] S. Schoder and K. Roppert, "openCFS: Open source finite element software for coupled field simulation – part acoustics," 2022.

[11] M. Kaltenbacher, *Numerical Simulation of Mechatronic Sensors and Actuators*. Springer, third ed., 2015.

[12] D. Lafarge, P. Lemarinier, J. F. Allard, and V. Tarnow, "Dynamic compressibility of air in porous structures at audible frequencies," *J. Acoust. Soc. Am.*, vol. 102, no. 4, pp. 1995–2006, 1997.

[13] S. Floss, F. Czwielong, M. Kaltenbacher, and S. Becker, "Design of an in-duct micro-perforated panel absorber for axial fan noise attenuation," *Acta Acust.*, vol. 5, p. 24, 2021.

[14] M. Möser, *Engineering Acoustics: An Introduction to Noise Control*. Springer Berlin, Heidelberg, second edition ed., 2009.

[15] MathWorks, "Matlab documentation: taylor()," 2023.

[16] E. Mušeljić, "PyCFS: Automatization and optimization interface library for trelis and cfs," 2023. v0.0.3, URL: `https://pypi.org/project/pycfs/`.

[17] M. Pastor, M. Binda, and T. Harčarik, "Modal assurance criterion," *Procedia Eng.*, vol. 48, pp. 543–548, 2012.